Applied Catalysis B: Environmental 148–149 (2014) 191–200

Contents lists available at ScienceDirect

Applied Catalysis B: Environmental

journal homepage: www.elsevier.com/locate/apcatb

Iron terephthalate metal–organic framework: Revealing the effective activation of hydrogen peroxide for the degradation of organic dye under visible light irradiation

Lunhong Ai, Caihong Zhang, Lili Li, Jing Jiang*

Chemical Synthesis and Pollution Control Key Laboratory of Sichuan Province, College of Chemistry and Chemical Engineering, China West Normal University, Nanchong 637002, PR China

ARTICLE INFO

Article history:
Received 17 July 2013
Received in revised form 26 October 2013
Accepted 27 October 2013
Available online 5 November 2013

Keywords:
Metal–organic framework
Heterogeneous catalysis
Hydrogen peroxide
Degradation
Electron transfer

ABSTRACT

Metal–organic frameworks (MOFs), a new class of porous crystalline materials, have attracted great interest as a promising candidate for sustainable energy and environmental remediation. In this study, we demonstrate that an iron terephthalate metal–organic framework MIL-53(Fe) synthesized by a facile solvothermal reaction was capable of activating hydrogen peroxide (H_2O_2) to achieve high efficiency in photocatalytic process. It could completely decompose the 10 mg L^{-1} Rhodamine B (RhB) in the presence of a certain amount of H_2O_2 under visible light irradiation within 50 min. The catalytic activities were found to be strongly affected by the various operating parameters, such as solution pH, initial dye concentration, and H_2O_2 dosage. The activation effects of MIL-53(Fe) were investigated through the detection of hydroxyl radicals (•OH) and transient photocurrent responses, which revealed that the H_2O_2 behaved in two ways during the catalytic process: (i) it could be catalytically decomposed by MIL(Fe)-53 to produce •OH radicals through the Fenton-like reaction; (ii) it could capture the photogenerated electrons in the conduction band of excited MIL-53(Fe) to form •OH radicals under visible light irradiation. The ability of such iron-based MOFs to activate H_2O_2 may enable rational design of advanced MOF-based catalysts for environmental remediation.

1. Introduction

Increasing global contamination of water body and deterioration of water quality has become a serious issue facing humanity in the current situation. The ever-increasing demand for clean water environment has triggered intense research on the advanced technology for water treatment. Among versatile physical, chemical, and biological technologies in pollution control, the advanced oxidation processes (AOPs), including Fenton reaction, photocatalysis, sonolysis, ozonation and their combination, are of great practical importance due to their high efficiency, simplicity, good reproducibility, and easy handling. AOPs generally involve an in situ generation of highly reactive and nonselective chemical oxidants such as hydroxyl radicals (•OH) to degrade the persistent and non-biodegradable organic substances [1,2]. In particular, the utilization of an environmentally benign oxidant, hydrogen peroxide (H_2O_2), to produce •OH has attracted considerable attention. Actually, H_2O_2 could decompose easily to •OH upon activation by transition metal ions (e.g., Fe^{2+}, Fe^{3+}, and Cr^{6+}) [3,4], inorganic bicarbonate ions [5,6], UV light irradiation and ultrasound irradiation. However, most of these approaches require rigorous operating pH range, long run times and increased energy consumption. Therefore, great research effort has been devoted to develop a heterogeneous solid catalyst system activating H_2O_2 to overcome the critical drawbacks of above homogeneous catalytic process. For example, iron-based heterogeneous Fenton-like catalysts have been explored as activation catalysts for H_2O_2, including Fe_3O_4 [7], α-FeOOH [8], $FeVO_4$ [9], $BiFeO_3$ [10], Fe alginate [11] and Fe-ZSM5 zeolite [12], to efficiently degrade organic dyes in aqueous solution. Meanwhile, recent studies have also shown that H_2O_2 could be activated by the semiconductor photocatalysts such as TiO_2, $BiVO_4$ [13], g-C_3N_4 [14], WO_3 [15], $K_3PW_{12}O_{40}$ [16], and $ZnFe_2O_4$ [17], facilitating to enhance the photocatalytic efficiency under visible light irradiation. Apparently, design and fabrication of the effective heterogeneous catalysts for H_2O_2 activation is a key issue to realize the desirable activity and long-term stability.

Metal–organic frameworks (MOFs) have emerged as an interesting class of multifunctional inorganic–organic hybrid porous crystalline materials, where metal ions or clusters are linked to organic linkers forming a three-dimensional well-defined structure, owing to their promising applications in gas storage, separation, catalysis, sensors and drug delivery [18–21]. Importantly,

* Corresponding author. Tel.: +86 817 2568081; fax: +86 817 2582029.
E-mail address: 0826zjjh@163.com (J. Jiang).

0926-3373/$ – see front matter © 2013 Elsevier B.V. All rights reserved.
http://dx.doi.org/10.1016/j.apcatb.2013.10.056

recent progress has shown that MOFs show an attractive semiconducting behavior that integrates different molecular functional components to achieve light harvesting and to photocatalytically drive various chemically useful reaction [22–24]. In contrast to the conventional semiconductor photocatalytic systems, photoactive MOF systems have advantages in solar harnessing more efficiently, as their structural features of tunable active sites (i.e., metal-oxo clusters and organic linkers), desirable porosity and high surface area allow not only for rational design and fabrication of the photocatalytic system at the molecular level, but also for fast transport and good accommodation of guest molecules. To this end, MOFs could serve as an ideal choice for light harvesting to achieve photocatalytic degradation of organic pollutions. For example, A MOF-5 behaves as a semiconductor upon light excitation for the generation of charge carriers (electrons and holes), which was able to photocatalytically degrade phenol in aqueous solutions [25]. A Cu-doped ZIF-67 has been used as a visible-light-driven photocatalyst for the degradation of methyl orange [24]. Chen et al. reported that a doubly interpenetrated semiconducting MOF UTSA-38 with a band gap of 2.85 eV exhibited photocatalytic activity for the degradation of methyl orange in aqueous solution [26]. Despite the great progress achieved so far, it is still essential to exploit high performance visible-light-responsive MOF-based photocatalysts.

Herein, we demonstrate the capability of an iron-based metal–organic framework MIL-53(Fe) for the activation of hydrogen peroxide (H_2O_2) to achieve high efficiency in visible light photocatalytic process. The photocatalytic rates of RhB degradation over MIL-53(Fe) were accelerate evidently with the assistance of H_2O_2. The activation mechanism of MIL-53(Fe) was investigated and proposed on the basis of experiment results of the detection of hydroxyl radicals and transient photocurrent responses, which confirm the enhanced photocatalytic activity could be arisen from the cooperative effects by combination of MIL-53(Fe) and H_2O_2 under visible light irradiation.

2. Experimental

2.1. Materials

$FeCl_3{\cdot}6H_2O$, terephthalic acid (1,4-BDC), dimethylformamide (DMF), Rhodamine B (RhB), H_2O_2 (30%, v/v), HCl and NaOH were purchased from Kelong Chemical Reagents Company (Chengdu, China) and used without further purification. All chemicals used in this study were of commercially available analytical grade.

2.2. Preparation of metal–organic framework MIL-53(Fe)

Metal–organic framework MIL-53(Fe) was prepared by a mild solvothermal process [27]. In a typical procedure, 1 mmol of $FeCl_3{\cdot}6H_2O$ and 1 mmol of 1,4-BDC were added slowly into 5 mL of DMF solution. The mixture was stirred for 10 min at room temperature, and then transferred into a Teflon-lined stainless steel autoclave with a volume capacity of 20 mL and heated at 150 °C for 2 h. After the heat treatment, the autoclave is allowed to cool naturally to room temperature, and the products are collected by centrifugation at 6000 rpm for 2 min. To remove the solvent, the obtained yellow powder was suspended into a 200 mL of distilled water overnight, and then centrifuged in water and dried in vacuum at 60 °C for 24 h.

2.3. Characterization

The powder X-ray diffraction (PXRD) measurements were recorded on a Rigaku Dmax/Ultima IV diffractometer with monochromatized Cu *K*α radiation (λ = 0.15418 nm). The morphology was observed with a JEOL JSM-6510LV scanning electron microscope (SEM). The elemental composition of the samples were characterized by energy-dispersive X-ray spectroscopy (EDS, Oxford instruments X-Max). The Fourier transform infrared (FTIR) spectroscopy was recorded on Nicolet 6700 FTIR Spectrometric Analyzer using KBr pellets. UV–vis diffused reflectance spectra of the samples were obtained for the dry-pressed film samples using a UV–vis spectrophotometer (UV-3600, Shimadzu, Japan). $BaSO_4$ was used as a reflectance standard in a UV–vis diffuse reflectance experiment. The Brunauer–Emmett–Teller (BET) surface area and porous structure were measured using an ASAP 2020 V3.01 H apparatus (Micromeritics Instrument Corp., USA). After the samples were degassed in vacuum at 120 °C for 6 h, the nitrogen adsorption and desorption isotherms were measured at 77 K.

2.4. Degradation experiments

The visible light photocatalytic degradation of RhB in the presence of H_2O_2 over MIL-53(Fe) was carried out in a cylindrical Pyrex vessel reactor. Typically, 0.01 g MIL-53(Fe) sample was added into 25 mL of RhB in a 100 mL cylindrical Pyrex vessel. Afterwards, suspension was mechanically stirred in the dark for 30 min to establish the adsorption/desorption equilibrium, followed by the addition of a known concentration of H_2O_2 to the mixture solution. The suspension was then illuminated by a 500 W halogen tungsten lamp through a UV-cutoff filter (420 nm). At predetermined time intervals, the suspension were extracted at different time intervals and then centrifuged to get the supernatant for analysis.

2.5. Analytical methods

The concentration of RhB left in the supernatant solution was determined by using a Shimadzu UV2550 UV–vis spectrophotometer at its maximum absorption wavelength of 554 nm. The pH of RhB solution was adjusted by adding aqueous solutions of 0.1 mol L^{-1} HCl or 0.1 mol L^{-1} NaOH, and determined by using a PHS-3C pH meter (Rex Instrument Factory, Shanghai, China). The formation of hydroxyl radicals (•OH) mediated by MIL-53(Fe) catalysts in the presence of H_2O_2 was detected by fluorescence method using terephthalic acid as a probe molecule [28]. The experimental procedures were similar to those used in the measurement of above catalytic experiments in the presence of H_2O_2 under visible light irradiation except that the aqueous solution of RhB was replaced by an aqueous solution of 0.5 mM terephthalic acid and 2 mM NaOH. The visible light irradiation was continuous and sampling was performed every 5 min for analysis with a RF-5301PC Shimadzu fluorescence spectrophotometer at 315 nm of excitation wavelength.

2.6. Electrochemical measurements

An electrochemical work station (CHI660D Instruments) connected to a computer was used in our electrochemical experiment. The electrodes were prepared according to Zhang's method [29]. For the preparation of the MOF electrodes, the MIL-53(Fe) were dispersed in chitosan solution to form a 10 mg mL^{-1} solution and ultrasonicated for 5 min, 0.3 mL of colloidal solution was dropped on the pretreated ITO surface and allowed to dry under vacuum conditions for 24 h at room temperature. The photocurrents were measured by an electrochemical analyzer in a standard three-electrode system with the MIL-53(Fe) as the working electrodes, a Pt foil as the counter electrode, and a saturated calomel electrode (SCE) as a reference electrode. A 500 W Xe arc lamp with a UV-cutoff filter (420 nm) was utilized as a light source. A 0.5 M Na_2SO_4 aqueous solution was used as the electrolyte. The Mott–Schottky measurements were carried out with impedance-potential model to evaluate the band positions of the MIL-53(Fe) catalyst.

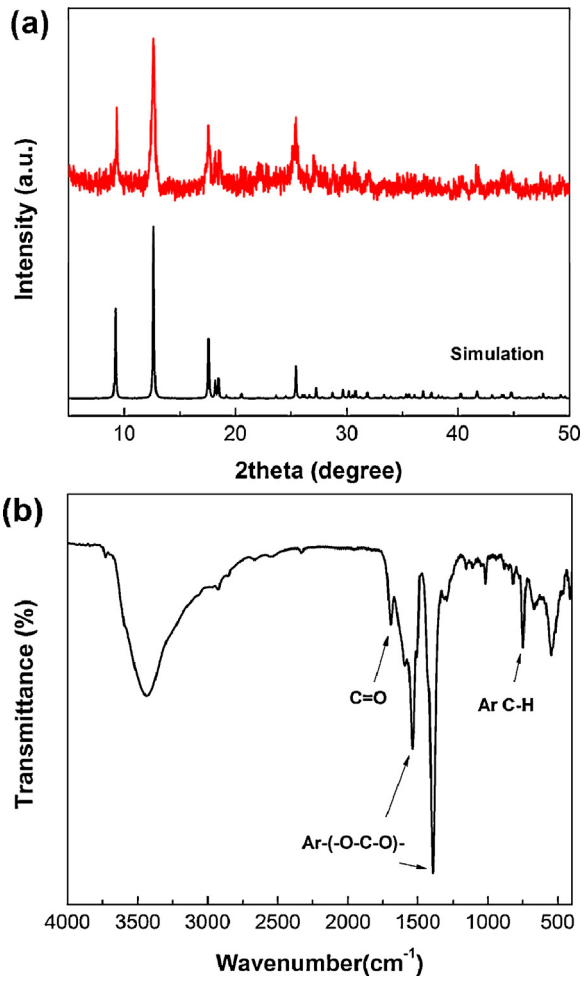

Fig. 1. (a) PXRD patterns of MIL-53(Fe) (red curve) and the simulated XRD pattern for the MIL-53 structure (black curve) created from CIF in reference documents [30]. (b) FTIR spectrum of MIL-53(Fe). (For interpretation of the references to color in this figure legend, the reader is referred to the web version of this article.)

3. Results and discussion

3.1. Characterization of the MIL-53(Fe) MOFs

The crystallographic structure of the as-prepared MIL-53(Fe) sample was examined by powder X-ray diffraction (PXRD). Fig. 1a displays a typical PXRD pattern of the MIL-53(Fe). Apparently, the well-defined diffraction peaks revealed the high crystallinity of the sample, which are in good agreement with the previously reported MIL-53 MOFs as well as the simulated one [30]. In order to deeply analyze the molecular structure and identify the functional groups of MIL-53(Fe) sample, the FTIR spectroscopy was performed and the result is shown in Fig. 1b. The characteristic absorption peaks of the MIL-53(Fe) sample were observed at 1680, 1543, 1396, 1020, and 750 cm^{-1}, which could mainly originate from the carboxylate groups vibrations and are identical to those of reported data in the literatures [31–33]. The broad peak centered at 3440 cm^{-1} is associated with the stretching vibrations of the O–H from the surface adsorbed water. The two sharp peaks at 1543 and 1396 cm^{-1} are assigned to asymmetric (ν_{as}(C–O)) and symmetric (ν_s(C–O)) vibrations of carboxyl groups, respectively, confirming the presence of the dicarboxylate linker within the sample. The peak at 750 cm^{-1} corresponds to C–H bending vibrations of the benzene. Therefore, the results of XRD analysis and FTIR spectra clearly confirm the formation of MIL-53(Fe) structure.

The morphology and particle size of the MIL-53(Fe) sample were observed by scanning electron microscopy (SEM). Fig. 2a is a low-magnification SEM image of the synthesized MIL-53(Fe). Clearly, two populations of particles was observed: one bigger rod-like crystals with a length of several micrometers and a width of 1–3 μm and other smaller pseudo-spherical particles having an average diameter of 300 nm, which are quite similar to the previously reported observation of MIL-53(Fe) by Horcajada et al. [27]. The magnified SEM image in Fig. 2b reveals that the smaller pseudo-spherical particles were tended to aggregate together, which were closely attached on the surface of the larger rod-like crystals. The compositional analysis carried out by energy-dispersive X-ray spectroscopy (EDS) measurements (Fig. 2c) shows the presence of Fe, C and O elements in the as-prepared MIL-53(Fe) sample. Moreover, the EDS elemental mapping (Fig. 3) further confirms that these elements were homogeneously distributed in the MIL-53(Fe).

Specific surface area and porous structure of MIL-53(Fe) determined by N_2 adsorption–desorption isotherms at 77 K. As shown in Fig. 4, the N_2 adsorption–desorption isotherms displayed an intermediate mode between type I and type IV, which is associated with mesoporous and microporous materials, respectively [34]. The Brunauer–Emmett–Teller (BET) surface area and total pore volume of MIL-53(Fe) were calculated to be 19.1 $m^2\ g^{-1}$ and 0.048 $cm^3\ g^{-1}$, respectively. The Barrett–Joyner–Halenda (BJH) mesopore size distribution curve exhibited a pore size centered at about 2.2 nm (Fig. 4b), while the micropore size was calculated to be about 0.62 nm from the Horvath–Kawazoe analysis (Fig. 4c).

The diffuse reflectance UV–vis spectroscopy of the MIL-53(Fe) sample was recorded. As shown in Fig. 5, the MIL-53(Fe) sample shows the strong absorption bands in the range of 200–400 nm. The characteristic absorption peaks were observed at around 240 and 290 nm, which can be assigned to absorption induced by ligand-to-metal charge transfer (LMCT) of O(II) → Fe(III) [35]. Clearly, the onset of the main absorption edge of MIL-53(Fe) was located at 430 nm. Based on the relation $E_g = 1240/\lambda$ [36], the calculated optical bandgap of MIL-53(Fe) is 2.88 eV (inset in Fig. 5). As expected, the prominent optical properties in UV–vis region of MIL-53(Fe) could contribute to an efficient photoreactivity.

3.2. Catalytic activity of the MIL-53(Fe)

The degradation of RhB was used to evaluate the catalytic performance of different systems, where control experiments were conducted to compare the removal efficiencies of RhB by various processes at natural pH (ca. 5.0) with initial RhB concentration of 10 mg L^{-1}. Fig. 6a shows the variation of RhB concentration (C/C_0) with reaction time during various processes. After visible light irradiation for 50 min, no observation of the photolysis of RhB in the absence of the catalyst reflects that the RhB was quite stable under visible light irradiation. While the presence of H_2O_2 could enhance the degradation efficiency of RhB up to 17.6% by photolysis process because of the possible H_2O_2 photolysis induced by incident light (H_2O_2 + visible light → •OH + OH^-). With MIL-53(Fe) alone under visible light irradiation, about 62.1% RhB removal was achieved, mainly due to the generation of reactive charge carriers by the excited photoactive MIL-53(Fe), indicating that the synthesized MIL-53(Fe) catalyst possessed moderate photoreactivity. Interestingly, after the addition of H_2O_2, the degradation efficiency of RhB over MIL-53(Fe) under visible light irradiation was remarkably enhanced; it could completely decompose the RhB within 50 min. The enhanced H_2O_2-mediated photocatalytic activity of MIL-53(Fe) can be clearly proven by the change of the UV–vis absorption spectra of the solution in the course of the RhB degradation (Fig. 6b). Considering the catalyst is iron-based terephthalate, the Fenton-like catalytic process could also induce the degradation of RhB after the addition of H_2O_2, we further

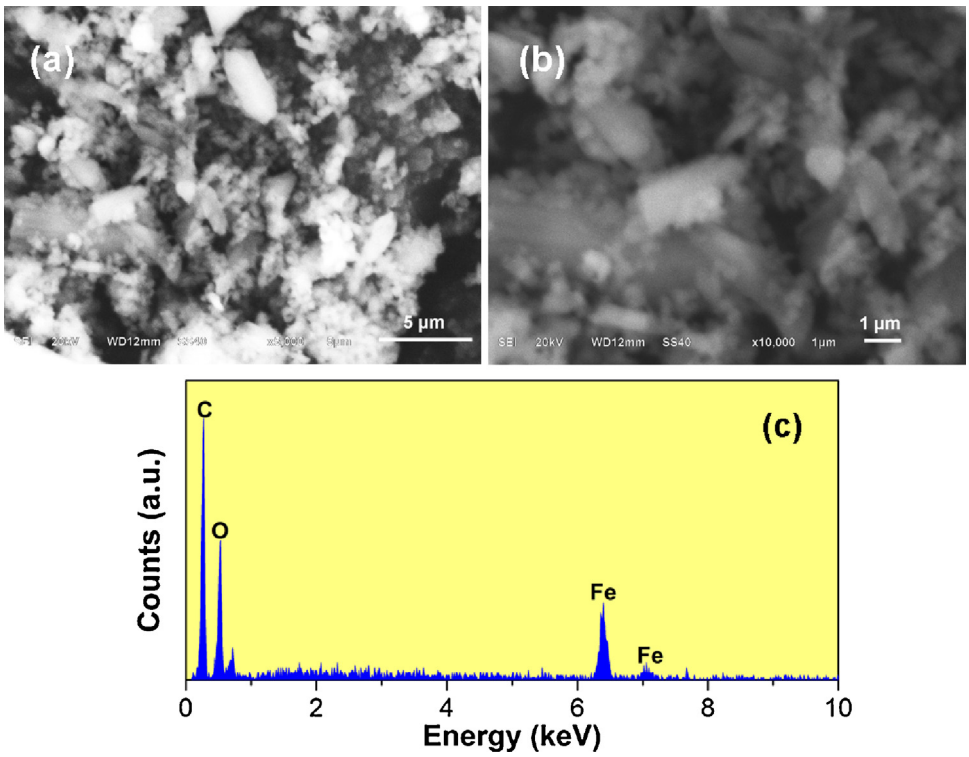

Fig. 2. SEM images ((a) and (b)) and EDS spectrum (c) of MIL-53(Fe).

carried out the control experiment in the dark by combination of H_2O_2 and MIL-53(Fe). As shown in Fig. 6a, about 58.1% of RhB were decomposed within 50 min, which suggests that MIL-53(Fe) indeed exhibited strong capability toward the activation of H_2O_2, thus driving the Fenton-like catalytic degradation of RhB; however, the efficiency in such Fenton-like catalytic process was relatively much lower than that in MIL-53(Fe)/visible light/H_2O_2 catalytic system. In addition, the degradation of RhB approximately followed pseudo-first-order kinetics, as evidenced by the linear plot of $\ln(C/C_0)$ vs. reaction time t (Fig. 6c). The kinetic enhancement of the catalyzed degradation of RhB (see Fig. 6d) over MIL-53(Fe) was more significant in the presence of both H_2O_2 and visible light (i.e., the MIL-53(Fe)/visible light/H_2O_2 system), based on the pseudo-first-order rate constants (7.94×10^{-2} min^{-1} for

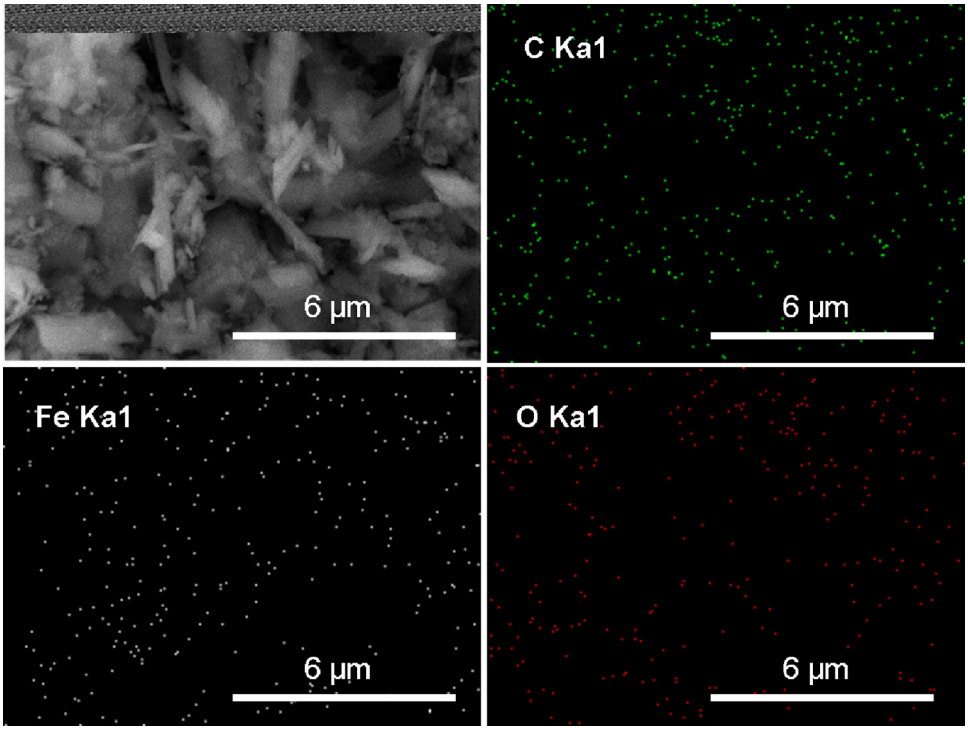

Fig. 3. EDS elemental mappings of MIL-53(Fe).

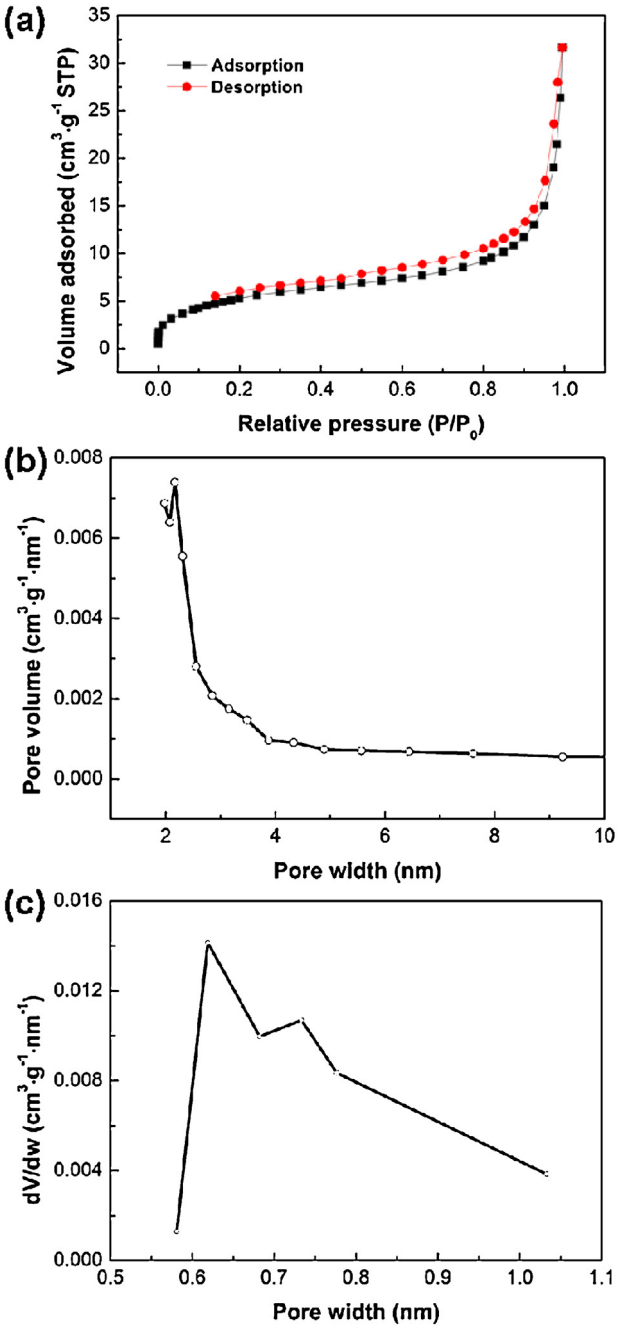

Fig. 4. (a) Nitrogen adsorption–desorption isotherms of MIL-53(Fe). (b) The Barrett–Joyner–Halenda (BJH) mesoporous size distribution of MIL-53(Fe). (c) The Horvath–Kawazoe (HK) micropore size distribution of MIL-53(Fe).

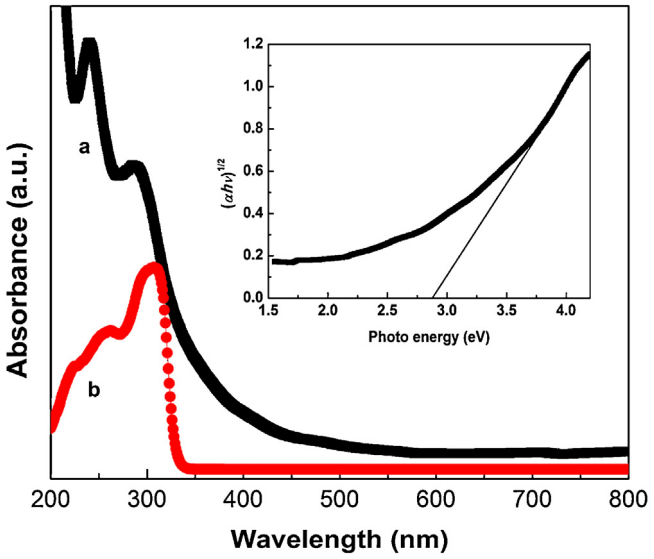

Fig. 5. UV–vis diffuse reflectance spectra of MIL-53(Fe) (a) and pure 1,4-BDC (b).

MIL-53(Fe)/visible light/H_2O_2; $1.83 \times 10^{-2}\,min^{-1}$ for MIL-53(Fe)/visible light; $1.74 \times 10^{-2}\,min^{-1}$ for MIL-53(Fe)/H_2O_2). Furthermore, the RhB degradation rate constant in the catalytic system of MIL-53(Fe)/visible light/H_2O_2 ($7.94 \times 10^{-2}\,min^{-1}$) was found to be even much higher than that of the sum of MIL-53(Fe)/visible light and MIL-53(Fe)/H_2O_2 catalytic systems ($3.57 \times 10^{-2}\,min^{-1}$), which suggests that the synergetic effect of the MIL-53(Fe) catalyst, H_2O_2 and visible light irradiation in the catalytic process could contribute cooperatively to the whole catalytic activity for the RhB degradation. Furthermore, we quantitatively evaluate the synergetic effect in the MIL-53(Fe)/visible light/H_2O_2 system by using the synergetic index (SI): $SI = k_{MVH}/(k_{MH} + k_{MV})$, where k_{MVH}, k_{MV}, and k_{MH} were the apparent rate constants in the catalytic systems of MIL-53(Fe)/visible light/H_2O_2, MIL-53(Fe)/visible light and MIL-53(Fe)/H_2O_2, respectively. The value of SI was obtained to be 2.22, implying this synergistic effect could enhance the catalytic activity of MIL-53(Fe) by 122%.

The solution pH is known to be an important factor that could remarkably affect the catalytic reaction. The effect of initial pH on the degradation efficiency of RhB over MIL-53(Fe)/visible light/H_2O_2 system was determined. As shown in Fig. 7, the MIL-53(Fe) catalyst could work effectively over a wide pH range from 3.0 to 9.0. This observation is consistent with the other catalytic systems of organometallic coordination polymers reported previously [37–39]; however, it is obviously different from the conventional or modified Fenton reaction usually performed at acidic condition. It is noticeable that the degradation rate of RhB decreased with the increase of pH from 5.0 to 9.0. This could be attributed to the fact that H_2O_2 is not stable in alkaline medium and tends to decompose to molecular oxygen and H_2O [40].

The effect of H_2O_2 dosage on RhB degradation over MIL-53(Fe)/visible light/H_2O_2 system was investigated by varying H_2O_2 concentration under a given reaction condition and the results are shown in Fig. 8. When H_2O_2 concentration increased from 5 to 20 mM, the degradation efficiency increased correspondingly from 77% to 98%. This enhancement in degradation rate is due to an increase in $^{\bullet}OH$ radicals with increasing the concentration of H_2O_2 [41,42]. However, increasing of H_2O_2 concentration from 20 to 40 mM, the degradation efficiency was not further enhanced but kept at an almost constant one. This can be explained that surplus H_2O_2 molecules act as scavenger of $^{\bullet}OH$ radicals to generate perhydroxy radicals with lower oxidation potential (Eqs. (1) and (2)) [43].

$$H_2O_2 + OH^{\bullet} \rightarrow H_2O + HOO^{\bullet} \quad (1)$$

$$HOO^{\bullet} + OH^{\bullet} \rightarrow H_2O + O_2 \quad (2)$$

The influence of initial dye concentration on the degradation of RhB over MIL-53(Fe)/visible light/H_2O_2 system was also evaluated. As shown in Fig. 9, the degradation efficiency of RhB was found to strongly depend on the initial dye concentration, which enhanced slightly with increasing initial dye concentration from 5 to 10 mg L^{-1}. The amount of RhB molecules per volume unit in solution increased by increasing the initial dye concentration, improving effectively contact between reactively oxidizing species

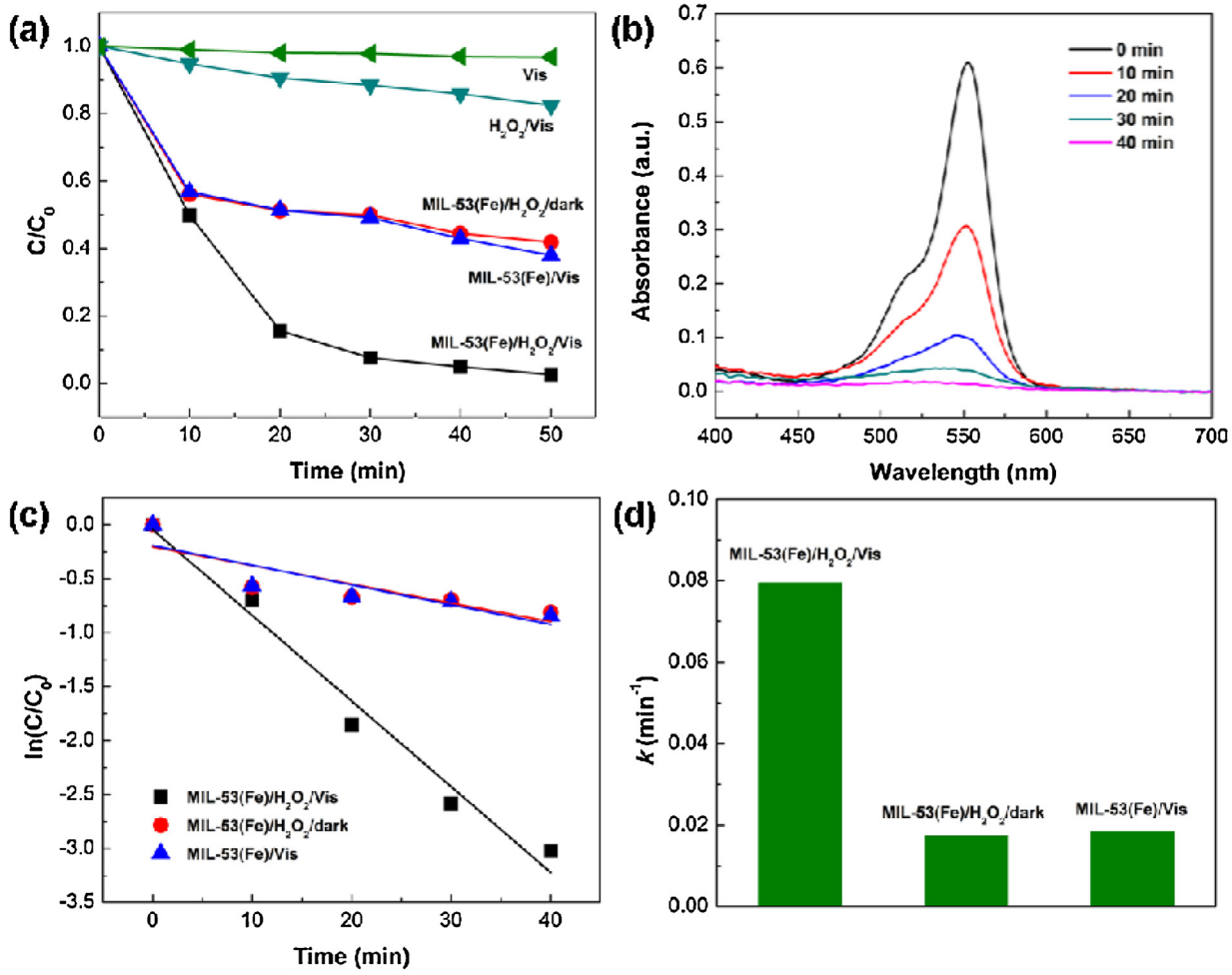

Fig. 6. (a) Degradation of RhB under different conditions. (b) The UV–vis spectral changes of RhB. (c) Pseudo-first-order kinetics curves of the degradation of RhB under different conditions. (d) Comparison of the apparent reaction rate constants of the degradation of RhB under different conditions. Experimental conditions: RhB, 10 mg L^{-1}; H_2O_2, 20 mM; MIL-53(Fe), 0.4 g L^{-1}; and initial pH 5.

and dye molecules, which could result in the enhancement of the degradation efficiency. However, the degradation efficiency was significantly decreased when the concentration of RhB increased from 10 to 25 mg L^{-1} because of a large molar extinction coefficient (88,000 cm^{-1} M^{-1}) RhB dye [44] leading to more impermeable solution to incident light, which results in the low efficiencies of light ulitization and low rates of photochemical processes.

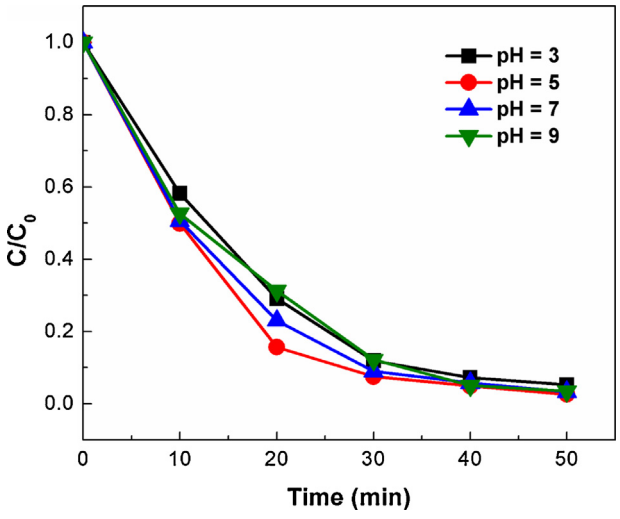

Fig. 7. Effect of initial pH on the degradation of RhB. Experimental conditions: RhB, 10 mg L^{-1}; H_2O_2, 20 mM; and MIL-53(Fe), 0.4 g L^{-1}.

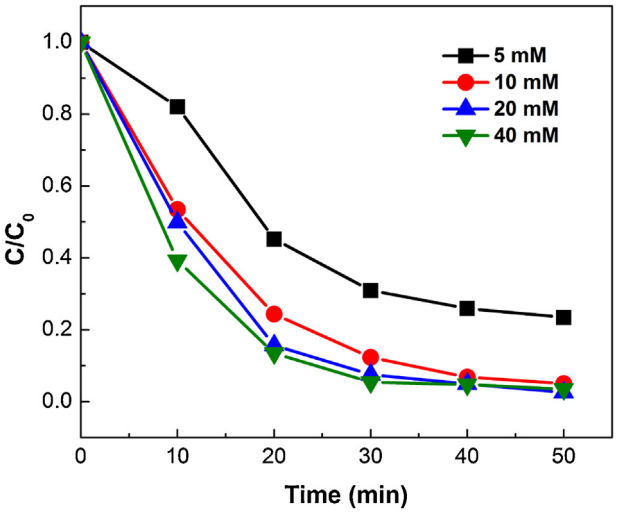

Fig. 8. Effect of H_2O_2 concentration on the degradation of RhB over MIL-53(Fe)/visible light/H_2O_2 system. Experimental conditions: RhB, 10 mg L^{-1}; MIL-53(Fe), 0.4 g L^{-1}; and initial pH 5.

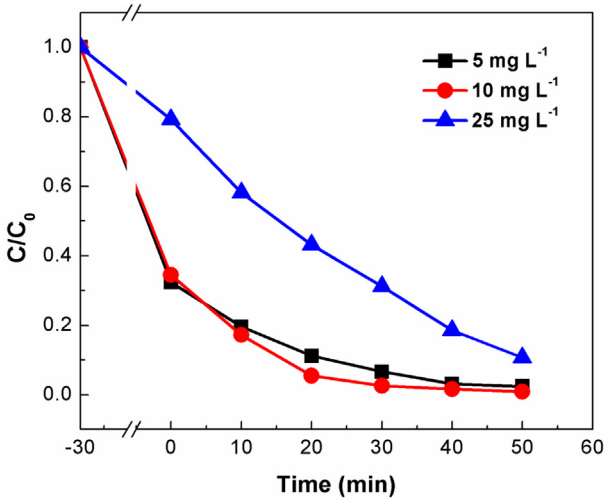

Fig. 9. Effect of initial dye concentration on the degradation of RhB over MIL-53(Fe)/visible light/H_2O_2 system. Experimental conditions: H_2O_2, 20 mM; MIL-53(Fe), 0.4 g L^{-1}; and initial pH 5.

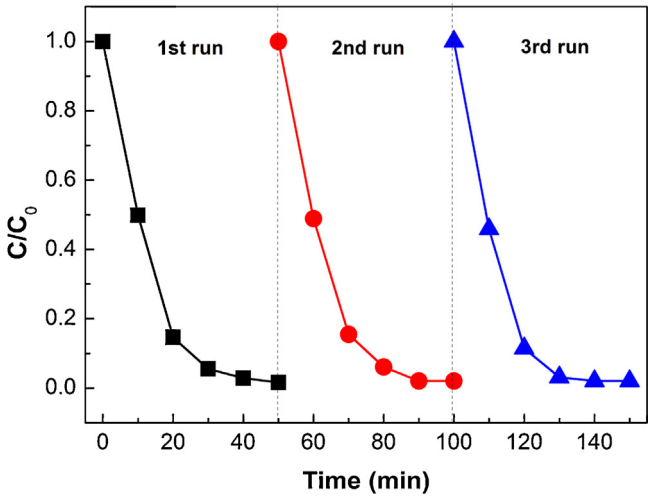

Fig. 10. The cycling runs of the degradation of RhB (10 mg L^{-1}) over MIL-53(Fe)/visible light/H_2O_2 system.

3.3. Reusability and stability of MIL-53(Fe)

The recyclability of MIL-53(Fe) was checked by circulating runs in the catalytic degradation of RhB over MIL-53(Fe)/visible light/H_2O_2 system. The results in Fig. 10 show that the catalytic oxidation performance of the MIL-53(Fe) catalyst remained almost unchanged after three recycles for the degradation of RhB, indicating that MIL-53(Fe) catalyst is very stable and can be used for repeated treatment of RhB dye. Also, MIL-53(Fe) almost kept its original yellow color after three recycles. Furthermore, the PXRD diffraction patterns and FTIR spectra of the used catalyst were found to be similar to that of fresh sample before reaction (Fig. 11 A and B), indicating there is no change in the chemical and crystal structure of the catalyst after three repeated reactions. These results

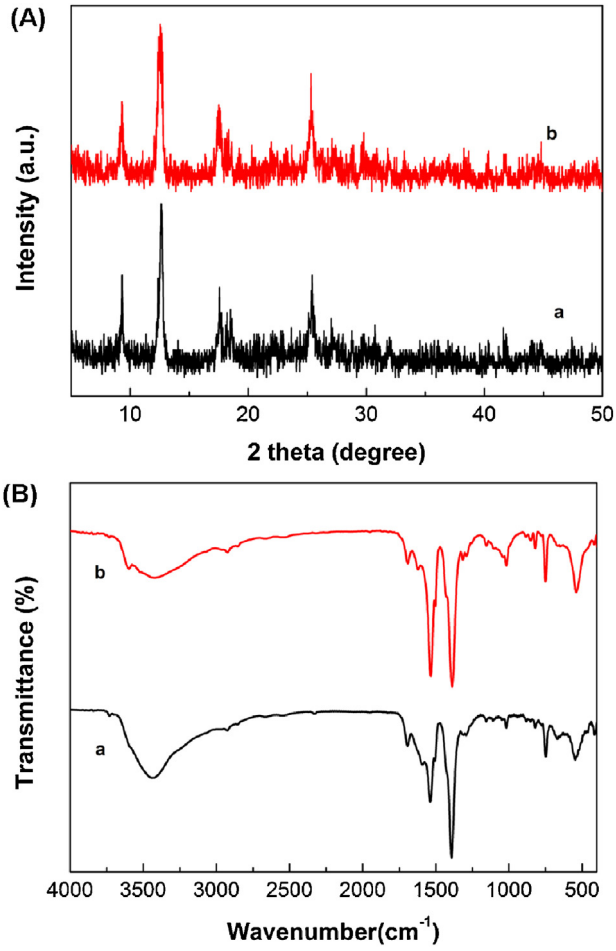

Fig. 11. PXRD patterns (A) and FTIR spectra (B) of MIL-53(Fe) before (a) and after (b) catalytic reaction.

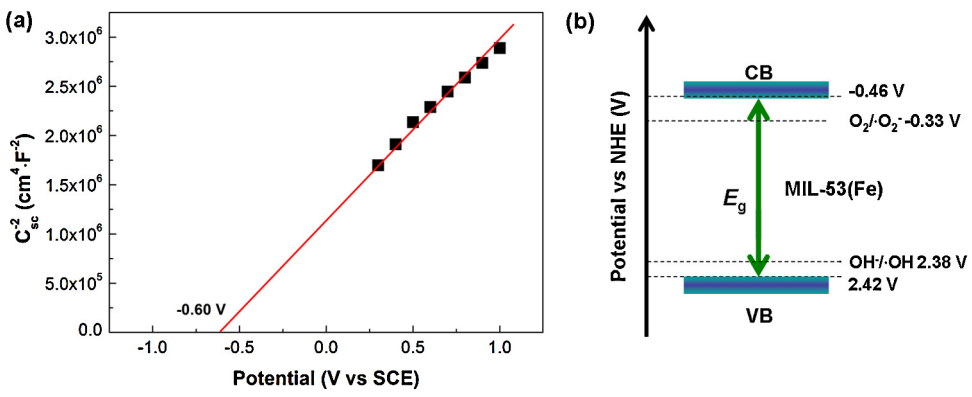

Fig. 12. (a) Mott–Schottky plots for the MIL-53(Fe) electrodes; (b) estimated energy level diagram of the MIL-53(Fe).

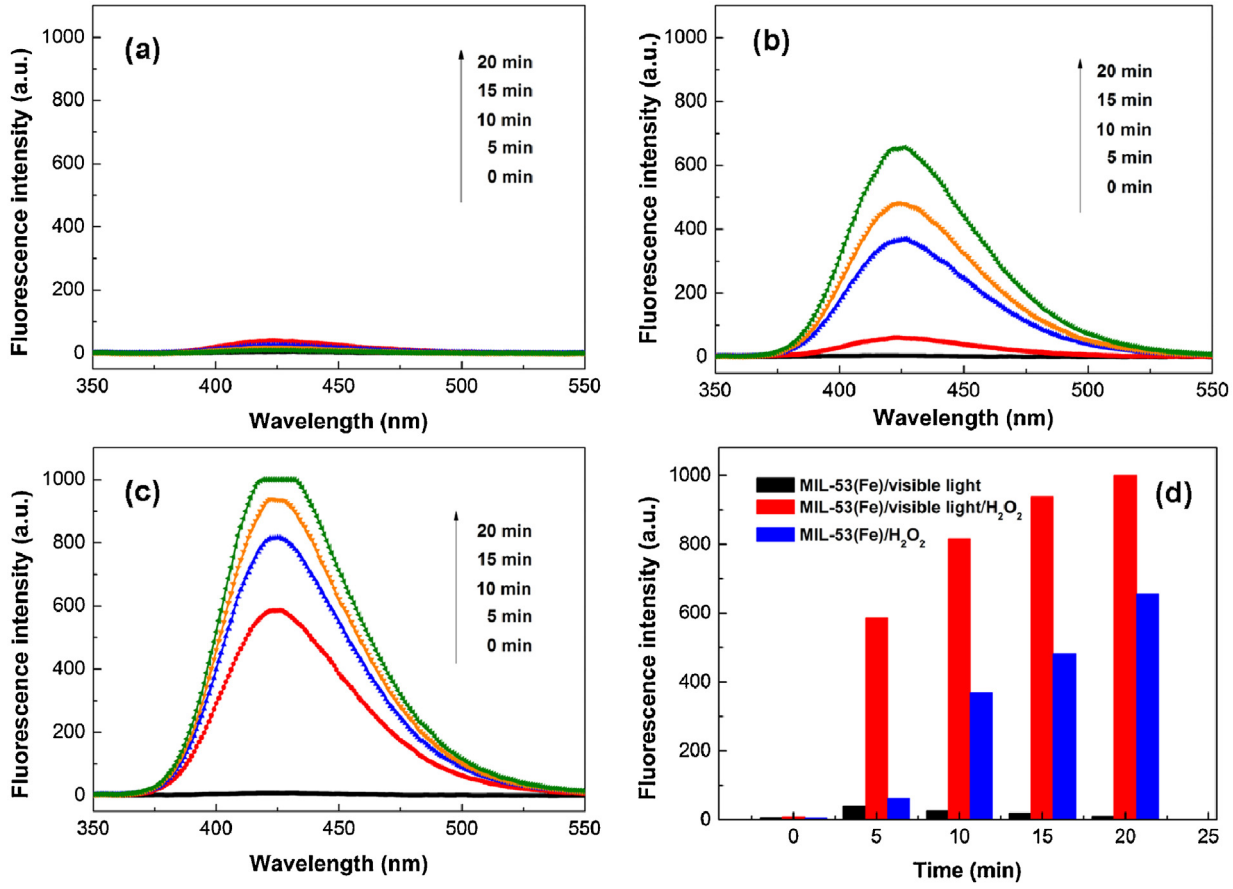

Fig. 13. •OH-trapping PL spectra of different catalytic systems: (a) MIL-53/visible light, (b) MIL-53(Fe)/H_2O_2 and (c) MIL-53(Fe)/visible light/H_2O_2. (d) Comparison of the PL intensities recorded every 5 min in catalytic systems of MIL-53/visible light and MIL-53(Fe)/H_2O_2 with MIL-53(Fe)/visible light/H_2O_2 catalytic system.

demonstrate that the presented MIL-53(Fe) catalyst was stable under the experimental reaction conditions employed here.

3.4. Mechanism for the RhB degradation in MIL-53(Fe)/visible light/H_2O_2 system

To understand the mechanism for the synergistic effect in MIL-53(Fe)/visible light/H_2O_2 system, we first evaluated the band positions of the MIL-53(Fe), which are intimately close to the redox ability of the photoinduced charge carriers. Fig. 12a shows a typical Mott–Schottky plot of the MIL-53(Fe) catalyst in the dark measured at a frequency of 100 Hz. The flatband potential of MIL-53(Fe) is determined to be −0.60 V vs. SCE (equivalent to −0.36 V vs. NHE). The conduction band (CB) of MIL-53(Fe) is therefore estimated to be −0.46 V vs. NHE, which is more negative than the redox potential of $O_2/{}^{\bullet}O_2^-$ (−0.33 V vs. NHE) and benefits the photogenerated electron transfer from catalyst to adsorbed molecular oxygen. Combined with the band gap energy estimated from UV–visible spectra, valence band (VB) of MIL-53(Fe) is calculated to be 2.42 V vs. NHE according to the empirical formula: $E_{CB} = E_{VB} - E_g$. As illustrated in Fig. 12b, MIL-53(Fe) is apparently not easy to oxidize OH^- to •OH radicals under visible light irradiation, because its VB value is very close to redox potential of $^{\bullet}OH/OH^-$ (2.38 V vs. NHE). Notably, the redox potential of RhB is about 1.43 V vs. NHE [45], which is significantly lower than VB level of MIL-53(Fe), indicating that the direct hole oxidation process is also energetically favorable. To support above hypothesis, we further employed the photoluminescence (PL) method to detect •OH radicals by reacting terephthalic acid with hydroxyl radical to produce highly fluorescent compound. As shown in Fig. 13a, in the MIL-53(Fe)/visible light system, unobservable PL means that •OH radicals were hardly generated in this catalytic system, indicating that the •OH radicals are not the main active oxygen species in the photochemical process of the MIL-53(Fe)/visible light system.

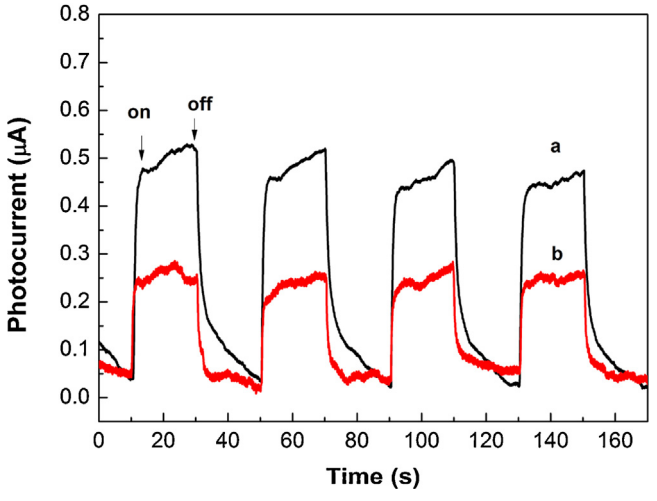

Fig. 14. Transient photocurrent responses of (a) MIL-53(Fe) and (b) MIL-53(Fe) with 70 mM H_2O_2 in 0.5 M Na_2SO_4 aqueous solutions under visible light irradiation.

As widely accepted, hydroxyl radicals (•OH) are the key active species in the H_2O_2-containing catalytic system, which have strong oxidative ability to attack most of stable organic molecules. The formation of •OH in the catalytic system of MIL-53(Fe)/visible

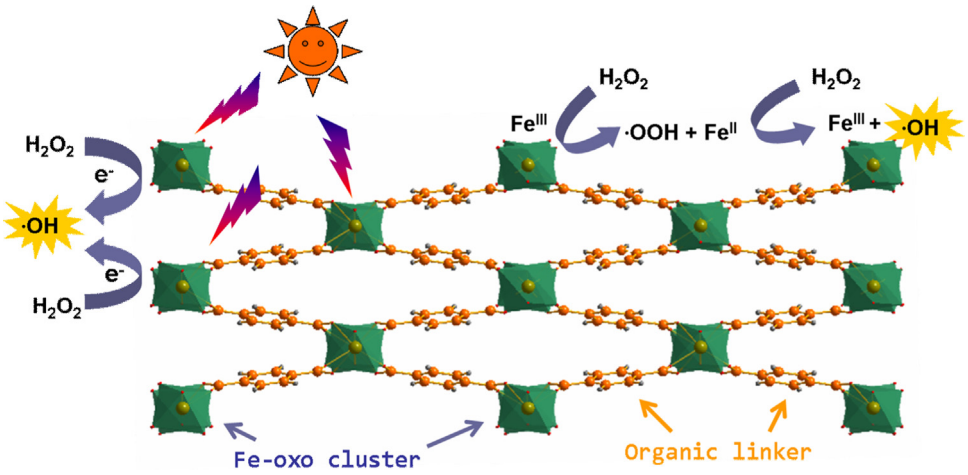

Fig. 15. Proposed mechanism for the activation of H_2O_2 by MIL-53(Fe) under visible light irradiation.

light/H_2O_2 was detected by PL method. For comparison, the MIL-53(Fe)/visible light and MIL-53(Fe)/H_2O_2 systems was also investigated under the same conditions. Fig. 13 shows the PL spectral changes observed in the different catalytic systems. In the case of MIL-53(Fe)/H_2O_2 system, a gradual increase in PL intensity at about 425 nm observed with increasing time confirms the production of •OH radicals, suggesting that MIL-53(Fe) can activate H_2O_2 to produce •OH radicals in the dark. It is very interesting that the PL intensity at about 425 nm increases sharply within 10 min observed in MIL-53(Fe)/visible light/H_2O_2 system. The strongest PL intensity in the MIL-53(Fe)/visible light/H_2O_2 system suggest more •OH radicals can be generated in such system, which should result from the existence of synergistic effects by combination of MIL-53(Fe) and H_2O_2 under visible light irradiation.

To further insight into the synergistic effects in the MIL-53(Fe)/visible light/H_2O_2 system, the transient photocurrent responses of the MIL-53(Fe) with H_2O_2 in solution under visible light irradiation were measured. Fig. 14 shows the photocurrent responses of different system under several on–off visible light irradiation cycles. Both systems were prompt in generating photocurrent with a reproducible response to on–off cycles. Interestingly, the photocurrent response of the MIL-53(Fe) is significantly reduced by the addition of H_2O_2, which indicates that H_2O_2 could react with photogenerated electrons to yield •OH radicals. This could be why the more •OH radicals generated in MIL-53(Fe)/visible light/H_2O_2 system than MIL-53(Fe)/H_2O_2 system, closely consistent with the above results of •OH-trapping PL spectra (Fig. 13).

Generally, there are two primary mechanisms for metal–organic framework during photocatalysis processes: (i) ligand-to-metal charge transfer (LMCT) mechanism [23,25,35,46] and (ii) metal–oxo cluster excitation [47–49]. As aforementioned, the pure organic linker (terephthalic acid) does not absorb any visible light, so the LMCT mechanism could be ruled out in our catalytic system. In this regard, it is reasonable to believe that the direct excitation of iron–oxo cluster is the main contributor to the photocatalytic performance of MIL-53(Fe), which has also been observed in recently reported iron(III)-based MOFs by Roeffaers et al. [47]. On the basis of this consideration, we therefore proposed the possible mechanism for the activation of H_2O_2 by MIL-53(Fe) under visible light irradiation. As illustrated in Fig. 15, the porous iron terephthalates MIL-53(Fe) structure is made of terephathalate anions and trans chains of Fe(III) octahedra sharing OH groups to generate a three-dimensional framework with a one-dimensional pore channel system [31]. Under visible light irradiation, the iron–oxo cluster in MIL-53(Fe) could adsorb incident photons, which is responsible for the visible light response and the associated photocatalytic activity. This could explain the photoactive characteristic of MIL-53(Fe). Importantly, in the presence of H_2O_2, the positive synergistic effects could contribute to the catalytic performance of MIL-53(Fe). On the one hand, Fe(III) on the surface of MIL-53(Fe) can catalyze the decomposition of H_2O_2 to produce •OH radicals by the Fenton-like reaction (Eqs. (3) and (4)).

$$\text{Fe(III)species} + H_2O_2 \rightarrow \text{Fe(II)species} + HO_2^{\bullet} + H^+ \quad (3)$$

$$\text{Fe(II)species} + H_2O_2 \rightarrow \text{Fe(III)species} + {}^{\bullet}OH + OH^- \quad (4)$$

On the other hand, H_2O_2 as an efficient scavenger could capture the photoinduced electrons in the excited MIL-53(Fe) to form •OH radicals (Eqs. (5) and (6)).

$$\text{MIL-53(Fe)} + h\nu \rightarrow h^+ + e^- \quad (5)$$

$$H_2O_2 + e^-_{(\text{MIL-53(Fe)})} \rightarrow {}^{\bullet}OH + OH^- \quad (6)$$

As expectedly, the above processes could cooperatively contribute to the activation of H_2O_2 by MIL-53(Fe) to produce more amounts of •OH radicals, thus greatly enhancing the degradation efficiency of RhB.

4. Conclusions

In summary, we have demonstrated that the iron-based MIL-53(Fe) metal–organic framework shows strong capability toward the activation of H_2O_2 to realize the highly efficient catalytic activity under visible light irradiation. The catalytic activities were closely dependent on the various operating parameters, such as solution pH, initial dye concentration, and H_2O_2 dosage. Interestingly, catalytic degradation of RhB proceeded about 4.3- and 4.6-fold faster in the MIL-53(Fe)/visible light/H_2O_2 system relative to the MIL-53/visible light system and MIL-53(Fe)/H_2O_2 system, respectively. This enhanced catalytic activity was considered to be arisen from the synergistic effects by combination of MIL-53(Fe) and H_2O_2 under visible light irradiation, which was confirmed by the results of detection of hydroxyl radicals (•OH) and transient photocurrent responses. This study provides new physical insights for the H_2O_2 activation by the photoactive iron-based catalysts and the rational design of advanced MOF-based catalysts for environmental remediation.

Acknowledgements

This work was supported by the National Natural Science Foundation of China (21103141 and 21207108), the Sichuan Youth Science and Technology Foundation (2013JQ0012), the Applied Basic Research Program of Sichuan Provincial Science and Technology Department (2011JYZ019) and the Research Foundation of CWNU (12B018).

References

[1] W. Liu, Z. Ai, L. Zhang, J. Hazard. Mater. 243 (2012) 257–264.
[2] Z. Ai, L. Lu, J. Li, L. Zhang, J. Qiu, M. Wu, J. Phys. Chem. C 111 (2007) 4087–4093.
[3] A. Bokare, W. Choi, Environ. Sci. Technol. 44 (2010) 7232–7237.
[4] W. Huang, M. Brigante, F. Wu, C. Mousty, K. Hanna, G. Mailhot, Environ. Sci. Technol. 47 (2013) 1952–1959.
[5] L. Zhou, W. Song, Z. Chen, G. Yin, Environ. Sci. Technol. 47 (2013) 3833–3839.
[6] X. Long, Z. Yang, H. Wang, M. Chen, K. Peng, Q. Zeng, A. Xu, Ind. Eng. Chem. Res. 51 (2012) 11998–12003.
[7] L. Xu, J. Wang, Appl. Catal., B 123-124 (2012) 117–126.
[8] Y. Zhao, J. Hu, Appl. Catal., B 78 (2008) 250–258.
[9] J. Deng, J. Jiang, Y. Zhang, X. Lin, C. Du, Y. Xiong, Appl. Catal., B 84 (2008) 468–473.
[10] W. Luo, L.H. Zhu, N. Wang, H.Q. Tang, M.J. Cao, Y.B. She, Environ. Sci. Technol. 44 (2010) 1786–1791.
[11] Y. Dong, W. Dong, Y. Cao, Z. Han, Z. Ding, Catal. Today 175 (2011) 346–355.
[12] M.B. Kasiri, H. Aleboyeh, A. Aleboyeh, Appl. Catal., B 84 (2008) 9–15.
[13] M. Ge, L. Liu, W. Chen, Z. Zhou, CrystEngComm 14 (2012) 1038–1044.
[14] Y. Cui, Z. Ding, P. Liu, M. Antonietti, X. Fu, X. Wang, Phys. Chem. Chem. Phys. 14 (2012) 1455–1462.
[15] H. Lee, J. Choi, S. Lee, S.-T. Yun, C. Lee, J. Lee, Appl. Catal., B 138-139 (2013) 311–317.
[16] C. Chen, Q. Wang, P. Lei, W. Song, W. Ma, J. Zhao, Environ. Sci. Technol. 40 (2006) 3965–3970.
[17] M. Su, C. He, V.K. Sharma, M.A. Asi, D. Xia, X.-Z. Li, H. Deng, Y. Xiang, J. Hazard. Mater. 211-212 (2012) 95–103.
[18] T. Watanabe, D.S. Sholl, Langmuir 28 (2012) 14114–14128.
[19] C. Wang, M. Zheng, W. Lin, J. Phys. Chem. Lett. 2 (2011) 1701–1709.
[20] S. Keskin, S. Kızılel, Ind. Eng. Chem. Res. 50 (2011) 1799–1812.
[21] M. Zheng, H. Tan, Z. Xie, L. Zhang, X. Jing, Z. Sun, ACS Appl. Mater. Interfaces 5 (2013) 1078–1083.
[22] J.-L. Wang, C. Wang, W. Lin, ACS Catal. 2 (2012) 2630–2640.
[23] T. Toyao, M. Saito, Y. Horiuchi, K. Mochizuki, M. Iwata, H. Higashimura, M. Matsuoka, Catal. Sci. Technol. 3 (2013) 2092–2097.
[24] H. Yang, X.-W. He, F. Wang, Y. Kang, J. Zhang, J. Mater. Chem. 22 (2012) 21849–21851.
[25] M. Alvaro, E. Carbonell, B. Ferrer, F.X. Llabrési Xamena, H. Garcia, Chem. Eur. J. 13 (2007) 5106–5112.
[26] M.C. Das, H. Xu, Z. Wang, G. Srinivas, W. Zhou, Y.-F. Yue, V.N. Nesterov, G. Qian, B. Chen, Chem. Commun. 47 (2011) 11715–11717.
[27] P. Horcajada, T. Chalati, C. Serre, B. Gillet, C. Sebrie, T. Baati, J.F. Eubank, D. Heurtaux, P. Clayette, C. Kreuz, J.-S. Chang, Y.K. Hwang, V. Marsaud, P.-N. Bories, L. Cynober, S. Gil, G. Ferey, P. Couvreur, R. Gref, Nat. Mater. 9 (2010) 172–178.
[28] X. Yu, J. Yu, B. Cheng, B. Huang, Chem. Eur. J. 15 (2009) 6731–6739.
[29] K. Zhao, X. Zhang, L. Zhang, Electrochem. Commun. 11 (2009) 612–615.
[30] F. Millange, N. Guillou, R.I. Walton, J.-M. Greneche, I. Margiolakid, G. Fereya, Chem. Commun. (2008) 4732–4734.
[31] P. Horcajada, C. Serre, G. Maurin, N.A. Ramsahye, F. Balas, M. Vallet-Regí, M. Sebban, F. Taulelle, G. Férey, J. Am. Chem. Soc. 130 (2008) 6774–6780.
[32] T. Devic, P. Horcajada, C. Serre, F. Salles, G. Maurin, B. Moulin, D. Heurtaux, G. Clet, A. Vimont, J.-M. Grenèche, B. Le Ouay, F. Moreau, E. Magnier, Y. Filinchuk, J. Marrot, J.-C. Lavalley, M. Daturi, G. Férey, J. Am. Chem. Soc. 132 (2010) 1127–1136.
[33] A. Banerjee, R. Gokhale, S. Bhatnagar, J. Jog, M. Bhardwaj, B. Lefez, B. Hannoyer, S. Ogale, J. Mater. Chem. 22 (2012) 19694–19699.
[34] L. Peng, J. Zhang, J. Li, B. Han, Z. Xue, G. Yang, Chem. Commun. 48 (2012) 8688–8690.
[35] Y. Fu, D. Sun, Y. Chen, R. Huang, Z. Ding, X. Fu, Z. Li, Angew. Chem. Int. Ed. 51 (2012) 3364–3367.
[36] J. Long, S. Wang, Z. Ding, S. Wang, Y. Zhou, L. Huang, X. Wang, Chem. Commun. 48 (2012) 11656–11658.
[37] S.E.-d.H. Etaiw, M.M. El-bendary, Appl. Catal., B 126 (2012) 326–333.
[38] H. Wang, Y. Huang, J. Hazard. Mater. 191 (2011) 163–169.
[39] M. Bazaga-Garcia, A. Cabeza, P. Olivera-Pastor, I. Santacruz, R.M.P. Colodrero, M.A.G. Aranda, J. Phys. Chem. C 116 (2012) 14526–14533.
[40] S. Zhang, X. Zhao, H. Niu, Y. Shi, Y. Cai, G. Jiang, J. Hazard. Mater. 167 (2009) 560–566.
[41] R. Idel-aouad, M. Valiente, A. Yaacoubi, B. Tanouti, M. López-Mesas, J. Hazard. Mater. 186 (2011) 745–750.
[42] M. Xia, M. Long, Y. Yang, C. Chen, W. Cai, B. Zhou, Appl. Catal., B 110 (2011) 118–125.
[43] Q. Chen, P. Wu, Y. Li, N. Zhu, Z. Dang, J. Hazard. Mater. 168 (2009) 901–908.
[44] Q. Jiang, A.-M. Spehar, M. Hakansson, J. Suomi, T. Ala-Kleme, S. Kulmala, Electrochim. Acta 51 (2006) 2706–2714.
[45] S.C. Yan, Z.S. Li, Z.G. Zou, Langmuir 26 (2010) 3894–3901.
[46] Y. Horiuchi, T. Toyao, M. Saito, K. Mochizuki, M. Iwata, H. Higashimura, M. Anpo, M. Matsuoka, J. Phys. Chem. C 116 (2012) 20848–20853.
[47] K.G.M. Laurier, F. Vermoortele, R. Ameloot, D.E. De Vos, J. Hofkens, M.B.J. Roeffaers, J. Am. Chem. Soc. 135 (2013) 14488–14491.
[48] P. Mahata, G. Madras, S. Natarajan, J. Phys. Chem. B 110 (2006) 13759–13768.
[49] Z.T. Yu, Z.L. Liao, Y.S. Jiang, G.H. Li, J.S. Chen, Chem. Eur. J. 11 (2005) 2642–2650.